HHS Public Access

Author manuscript

Biomaterials. Author manuscript; available in PMC 2021 February 01.

Published in final edited form as:

Biomaterials. 2020 February ; 230: 119634. doi:10.1016/j.biomaterials.2019.119634.

Cell-mediated matrix stiffening accompanies capillary morphogenesis in ultra-soft amorphous hydrogels

Benjamin A. Juliar[1,*], **Jeffrey A. Beamish**[2,*], **Megan E. Busch**[1], **David S. Cleveland**[2], **Likitha Nimmagadda**[1], **Andrew J. Putnam**[1]

[1]Department of Biomedical Engineering, University of Michigan, Ann Arbor, Michigan

[2]Division of Nephrology, Department of Internal Medicine, University of Michigan, Ann Arbor, Michigan

Abstract

There is a critical need for biomaterials that support robust neovascularization for a wide-range of clinical applications. Here we report how cells alter tissue-level mechanical properties during capillary morphogenesis using a model of endothelial-stromal cell co-culture within poly(ethylene glycol) (PEG) based hydrogels. After a week of culture, we observed substantial stiffening in hydrogels with very soft initial properties. Endothelial cells or stromal cells alone, however, failed to induce hydrogel stiffening. This stiffening tightly correlated with degree of vessel formation but not with hydrogel compaction or cellular proliferation. Despite a lack of fibrillar architecture within the PEG hydrogels, cell-generated contractile forces were essential for hydrogel stiffening. Upregulation of alpha smooth muscle actin and collagen-1 was also correlated with enhanced vessel formation and hydrogel stiffening. Blocking cell-mediated hydrogel degradation abolished stiffening, demonstrating that matrix metalloproteinase (MMP)-mediated remodeling is required for stiffening to occur. These results highlight the dynamic reciprocity between cells and their mechanical microenvironment during capillary morphogenesis and provide important insights for the rational design of materials for vasculogenic applications.

---

[*]contributed equally to this work

CRediT author statement:

Benjamin A. Juliar: Conceptualization, Methodology, Software, Validation, Formal Analysis, Investigation, Writing—Original Draft, Writing—Review & Editing, Visualization.

Jeffrey A. Beamish: Conceptualization, Methodology, Validation, Formal Analysis, Investigation, Resources, Writing—Original Draft, Writing—Review & Editing, Visualization.

Megan E. Busch: Investigation.

David S. Cleveland: Software, Investigation.

Likitha Nimmagada: Investigation.

Andrew J. Putnam: Conceptualization, Resources, Writing—Review & Editing, Project Administration, Funding Acquisition.

DATA AVAILABILITY STATEMENT

All data required to reproduce these findings are available from the corresponding author upon request.

Declaration of interests

The authors declare that they have no known competing financial interests or personal relationships that could have appeared to influence the work reported in this paper.

Keywords

Capillary morphogenesis; mechanical properties; hydrogel; poly(ethylene glycol); matrix metalloproteinase

INTRODUCTION

Biomaterials that support capillary formation are critical for wide ranging regenerative medicine applications [1, 2]. To date, most studies of 3D capillary morphogenesis have used biologically-derived extracellular matrix (ECM) hydrogels such as fibrin, collagen and Matrigel [3]. Synthetic, proteolytically degradable poly(ethylene glycol) (PEG) hydrogel ECMs also have attracted interest because of their biocompatibility and versatile macromer chemistry [4]. However, the extent of capillary morphogenesis is significantly restricted in PEG hydrogels compared with biologically-derived ECMs [5–7]. To overcome this limitation, a range of strategies have emerged to modulate initial hydrogel properties [8, 9] and to incorporate proangiogenic biological cues into PEG hydrogels to enhance their angiogenic potential [7, 10–12]. Despite this interest, relatively few studies have investigated how cellular remodeling of these minimalist PEG matrices accompanies microvascular morphogenesis [8].

Biophysical and biochemical cues in the ECM guide cellular remodeling, which in turn, alters the mechanical and biochemical microenvironment [13]. This dynamic and reciprocal relationship between cells and their ECM occurs throughout capillary morphogenesis. While many biochemical cues have been established [14], the relationship between microvascular cells and their mechanical microenvironment also plays a critical role. In fibrillar ECMs, mechanical tension helps guide endothelial migration and sprouting [15, 16] and fiber recruitment plays an important role in this process both in 2D [17] and 3D [18]. Stiffening of initially soft fibrillar hydrogels occurs both locally and globally as capillary morphogenesis proceeds [18, 19]. However, whether soft or stiff fibrillar ECMs best support vessel formation depends on the model system used [20].

In PEG hydrogels, the pericellular microenvironment has an amorphous nano-scale architecture that is distinct from fibrillar ECMs [21] which alters how force transmission occurs. In contrast to conflicting reports regarding stiffness effects in fibrillar ECMs, in PEG hydrogels capillary morphogenesis is inversely related to initial modulus [6, 8, 12, 22]. Though differences in matrix degradability [23] and diffusion [6] likely contribute to these effects, whether cell-mediated mechanical cues contribute to enhanced capillary morphogenesis in these soft amorphous matrices, which lack the fibrous architecture needed to support long-range force propagation, remains poorly understood. Moreover, whether cell-mediated matrix stiffening occurs in amorphous PEG hydrogels and associates with capillary morphogenesis is unknown.

To address these questions, we generated PEG hydrogels with a range of initial moduli and measured how the extent of capillary morphogenesis and bulk stiffening correlated. Using this model, we then interrogated the relative contributions of cell generated traction, ECM deposition, and cell-mediated remodeling on stiffening behavior to better understand the

mechanisms underpinning cell-mediated changes to hydrogel mechanics and enhanced capillary morphogenesis in soft amorphous hydrogels.

MATERIALS AND METHODS

Cell culture

All reagents were obtained from Thermo Fisher Scientific (Waltham, MA) unless specified. Endothelial and stromal cell sources in this study were chosen to provide continuity with our prior work [5, 19]. Human umbilical vein endothelial cells (ECs) were harvested from fresh umbilical cords (obtained from the University of Michigan's Mott's Children's Hospital via an IRB-exempt process, without any identifying information provided to the researchers) and cultured in fully supplemented Vasculife VEGF Endothelial Medium (Lifeline Cell Technology LLC, Frederick, MD) as previously described [24]. ECs were used between passages 2-4. Normal human dermal fibroblasts (DFs, Lonza, Walkersville, MD) were cultured in Dulbecco's modified Eagle medium (DMEM, Life Technologies, Grand Island, NY) supplemented with 10% fetal bovine serum (FBS, Life Technologies) and 1% penicillin streptomycin (Life Technologies) and were used up to passage 15. Both cell types were cultured at 37 °C and 5% CO_2 with thrice weekly medium exchanges. Cells were harvested below 80% confluence using 0.05% trypsin-EDTA (Life Technologies).

PEG-VS hydrogel formation.

Hydrogels were formed from 4-arm poly(ethylene glycol) vinyl sulfone (PEG-VS; 20 kDa, Jenkem USA, Allen TX) and a combination of a thiol containing adhesive peptide and a protease-sensitive crosslinking peptide adapted from published protocols [6, 25]. Hydrogels were functionalized with CGRGDS peptide ("RGD", Genscript, Piscataway, NJ) and crosslinked with Ac-GCRDVPMS↓MRGGDRCG-NH2 ("VPMS", Genscript, cleavage site indicated by ↓), which contains an N-terminal acetylation and a C-terminal amidation. These peptides were chosen to provide continuity with our previous work [5]. All reagents were prepared in batches of single-use aliquots. Peptides, dissolved in 25 mM acetic acid, and PEG-VS, dissolved in ultrapure water, were 0.22 μm filtered, lyophilized, and stored desiccated at −20 °C. Precise thiol content of each batch of peptide aliquots was determined using Ellman's reagent. Immediately before use, all reagents were dissolved in HEPES (100 mM, pH 8.4) to achieve final desired concentrations. RGD was reacted with the PEG-VS for 30 min to achieve a constant final concentration of 400 μM for all gel formulations. After RGD conjugation, VPMS was added to the PEG-VS solution, gently mixed, and 50 μl samples were dispensed into sterile 1 mL syringes with the needle end cut off. Hydrogels polymerized for 1 h at 37 °C in a sealed 50 mL conical tube. Polymerized hydrogels were punched into phosphate buffered saline (PBS). An optimal thiol:vinyl sulfone ratio (typically 0.8-0.9), achieved by varying crosslinker concentration to yield the maximum hydrogel shear modulus for acellular hydrogels, was determined for each batch and used for subsequent vasculogenesis assays.

Vasculogenesis assays and drug inhibitor studies

A 3D co-culture model of vasculogenesis, in which endothelial and stromal cells distributed in a hydrogel matrix self-assemble into a vascular network, was used as previously described

[5]. Briefly, hydrogels were formed as above except that a cell pellet was resuspended just before adding the crosslinking peptide to achieve a final cell seeding density of 2×10^6 cells/mL of each cell type (1×10^5 ECs and/or 1×10^5 DFs per 50 μl gel). Hydrogels were formed with 27, 32, and 40 mg/mL PEG-VS corresponding to 2.7%, 3.2%, and 4% (w/v PEG-VS). For quantification of gel compaction, a solution of Fluoresbrite Polychromatic Red microspheres (2.1 ± 0.018 μm diameter, 2.6% solids, Polysciences Inc, Warrington, PA) was additionally incorporated into hydrogels by substituting a 5% volume of HEPES for microsphere solution. Samples of the resulting suspension were dispensed and polymerized as above. Each hydrogel was cultured in 2 mL Vasculife VEGF medium in a 12-well plate for 7 d. For most conditions, medium was exchanged on days 1, 3, and 5. Blebbistatin (Calbiochem) and GM6001 (Calbiochem) were delivered in a 500x dilution of DMSO vehicle. Blebbistatin was delivered at a final concentration of 30 μM for all conditions and GM6001 was delivered to achieve the indicated final concentrations. 24-hour exposure to blebbistatin was achieved by spiking it into the culture media on day 6 of culture. Daily exposures to blebbistatin and GM6001 were achieved by exchanging culture media and inhibitors daily to maintain vehicle concentrations and inhibitor activities. All inhibitor conditions were compared to their appropriate vehicle controls. Experiments with 24-hour exposure to blebbistatin were performed with both 27 mg/mL and 32 mg/mL PEG hydrogels. Experiments in which blebbistatin and GM6001 were included throughout culture were performed with 32 mg/mL PEG hydrogels.

Mechanical characterization of PEG-VS hydrogels

Hydrogel shear moduli were obtained for all conditions on day 1 after allowing for hydrogel swelling and on day 7. Hydrogels were mounted on an AR-G2 rheometer (TA Instruments, New Castle, DE) between an 8-mm measurement head and a Peltier stage, each covered with P800 sandpaper. Shear storage modulus (G') was determined at 0.05 N normal force, 5% strain amplitude, and 1 rad/sec frequency and averaged over a 1-minute time sweep.

Fluorescent image quantification methods—On day 7, co-cultures were fixed with Z-fix (Anatech, Battle Creek, MI). All PEG-VS hydrogels were cut longitudinally down the cylinder midline prior to staining, yielding two halves. For quantification of vessel and nuclei density and cell spreading, samples were stained with rhodamine-conjugated lectin from *Ulex europaeus* (UEA, Vector Laboratories, Burlingame, CA, specific for endothelial cells, 1:200), 4', 6-diamidino-2-phenylindol (DAPI, 1 μg/mL, Sigma), and AlexaFluor 488 phalloidin (1:200). PEG-hydrogels were imaged on the cut side to ensure images were representative of cellular behavior within the hydrogels. Images were acquired using an Olympus IX81 microscope equipped with a disk scanning unit (DSU, Olympus America, Center Valley, PA) and Metamorph Premier software (Molecular Devices, Sunnyvale, CA). For all analyses, confocal z-stacks were acquired using the DSU. Z-series were collapsed into maximum intensity projections prior to analyses. Quantifications of vessel and nuclei densities were performed on 300 μm stacks (30 μm/slice) imaged at 4x (2.16 x 1.65 mm). Total vessel length per region of interest (ROI) was quantified from UEA images using the Angiogenesis Tube Formation module in Metamorph and reported as vessel length per volume of ROI. Total nuclei per ROI were quantified from DAPI images using a custom ImageJ script as previously described [5], and reported as counts per volume. A custom

ImageJ script (script and example included in supplement) was used to determine the fraction of UEA-negative nuclei. Briefly, binary DAPI projections were masked with their associated binary UEA projections and the fraction of DAPI stained area excluded from UEA-stained regions was calculated. Cell body circularity and projected cell area per volume of ROI were quantified from 30 μm thick stacks (3 μm/slice) of phalloidin images acquired at 10x (0.86 x 0.65 mm) and processed with a custom ImageJ script (included in supplement). Microbead density, as a measure of gel compaction, was calculated from 10 μm thick stacks (1 μm/slice) imaged at 20x (0.44 x 0.34 mm). Bead densities on day 0 were acquired before gel swelling. For each independent experiment, a value for each metric was determined by averaging multiple ROIs (4 for vessel and nuclei density, 6 for cell coverage and circularity, and 12 for bead densities). Only the final value of each parameter from each independent experiment (N=3-7) was subsequently analyzed in our statistical analysis.

Immunofluorescent staining and imaging

Following tissue construct fixation and bisection, hydrogels were permeabilized with 0.5% v/v TritonX-100 in tris-buffered saline (TBS) for 30 minutes then blocked overnight at 4°C in TBS with 2% w/v bovine serum albumin (BSA, Sigma-Aldrich) and 0.1% v/v Tween 20. Primary antibodies for alpha smooth muscle actin (Abcam, mouse IgG_{2b} isotype, 1:200 dilution), collagen-1 (Santa Cruz Biotech, mouse IgG_1 isotype, 1:200 dilution), fibronectin (Santa Cruz Biotech, mouse IgG_{2b} isotype, 1:200 dilution), collagen-IV (Invitrogen, mouse IgG_1 isotype, 1:500 dilution), or laminin beta-1 (Invitrogen, rabbit IgG, 1:500 dilution) were incubated with samples overnight at 4°C. Samples were then washed several times and incubated overnight at 4°C with appropriate secondary antibodies (Invitrogen, either AlexaFluor 488 goat-anti-mouse IgG_{H+L} or goat-anti-rabbit IgG_{H+L}, 1:200 dilutions). Samples were again washed then stained with DAPI and either UEA or AlexaFluor 568 phalloidin as indicated and stored in TBS. Representative images were acquired at 10x and 20x magnification using the DSU and presented as maximum intensity projections of 30 μm thick stacks (3 μm/slice).

Gene expression analysis

Hydrogels (2-3 per experimental replicate, pooled) were rinsed in PBS, cut into 4 pieces per gel, and incubated under constant gentle rotation in Collagenase IV (200 U/mL) at 37 °C for 30-40 min until gels were dissociated. The suspension was centrifuged at 500 × *g* for 3 min. The resulting cell pellet was lysed and RNA purified using an RNeasy Mini Kit (Qiagen, Venlo, Netherlands). RNA was reverse transcribed to cDNA using a High Capacity cDNA Reverse Transcription Kit (Applied Biosystems, Thermo Fisher Scientific). PCR amplifications were performed on a 7500 Fast Real-Time PCR System (Applied Biosystems) using Taqman Gene Expression reagents (20 ng cDNA per PCR reaction). The primer probe sets for the following genes were utilized (Taqman Assay ID indicated): GAPDH (Glyceraldehyde 3-phosphate dehydrogenase, Hs04420566_g1); TGFB1 (transforming growth factor β1, Hs00998133); PDGFRB (platelet derived growth factor receptor-β, Hs01019589_m1); PDGFB (platelet derived growth factor-β, Hs00966522_m1); ANTXR2 (capillary morphogenesis gene 2 protein, Hs00292467_m1); KDR (vascular endothelial growth factor receptor 2, Hs00911700_m1); ACTA2 (α-smooth muscle actin, Hs00426835_g1); COL1A1 (Collagen I, alpha 1 chain, Hs00164004_m1); LAMB1

(Laminin, Beta 1 chain, Hs01055960_m1); FN1 (Fibronectin 1, Hs01549976_m1); COL4A1 (Collagen IV, alpha 1 chain, Hs00266237_m1); MMP2 (matrix metalloproteinase 2, Hs01548724_m1); MMP9 (matrix metalloproteinase 9, Hs00957562_m1); MMP14 (membrane type 1 matrix metalloproteinase, Hs01037009_g1). The $\Delta\Delta C_t$ method was used to determine relative gene expression with GAPDH as the internal control.

Statistics

Statistical analysis was performed using GraphPAD Prism (La Jolla, CA). Unless noted, data are represented as mean ± standard deviation of at least 3 independent experiments. Data were analyzed using one- or two-way ANOVA with Tukey post-hoc testing with matching when possible and pre-specified comparisons between conditions on a given day and between days for a given condition. Correlations were determined by linear regression and R^2 and p value for the correlation coefficient reported. Statistics for gene expression data was performed in the C_t domain. A value of $\alpha < 0.05$ was considered significant.

RESULTS

1) Vessel density and hydrogel stiffening both depend on initial PEG composition and are tightly correlated

We first confirmed that initial PEG composition affects cellular morphogenetic processes including vessel formation, changes in cell density, and cell spreading consistent with previous work with EC-DF co-cultures [5]. We then characterized the expression of pro-angiogenic genes and the evolution of tissue-level physical properties including stiffening and compaction depending on PEG composition. Lower PEG concentration at gel polymerization supported increased vessel density at 7 d (Figure 1A and 1D), with a 2-fold higher vessel density in 27 mg/mL gels compared with 40 mg/mL ($p < 0.001$). The baseline shear moduli of hydrogels formed from 27, 32, and 40 mg/mL PEG were 59 ± 27 pa, 114 ± 27 pa, and 209 ± 50 pa, respectively (Figure 1B), confirming that changes in PEG composition led to differences in bulk shear storage moduli on day 1 (after swelling). These PEG densities were empirically chosen to interrogate the softest formulation which would consistently gel (27 mg/mL), the softest formulation which did not exhibit any stiffening behavior (40 mg/mL), and an intermediate formulation (32 mg/mL). Despite significant differences in vessel formation, we did not observe composition dependent differences in gene expression for a panel of angiogenesis-associated genes (Figure S1 A–E). After 7 d, 27 mg/mL hydrogels stiffened 2.7-fold ($p < 0.01$) and 32 mg/mL hydrogels stiffened 1.5-fold (NS), while the shear moduli of 40 mg/mL gels remained unchanged. Cell density did not vary with PEG composition at 1 d or 7 d, though there was a modest ~1.4-fold increase in total cell density for all gel compositions over the 7 d culture (Figure 1C, Figure S2, Two-way ANOVA: time $p < 0.001$, PEG $p > 0.99$, interaction $p = 0.60$). Cell density after 1 d was ~1.4×10^6 cell/mL (compared with 4×10^6 cell/mL at seeding), reflecting swelling of the gels after casting. There was a strong inverse correlation of the shear storage modulus at 1 d with vessel density at 7 d (Figure S3A, $R^2 = 0.762$, $p < 0.0001$), but no correlation with cell density (Figure S3B, $R^2 = 0.002$, $p = 0.956$). We noted a positive correlation between the degree of stiffening observed in each experiment and the ultimate vessel density at 7 d (Figure S3C, $R^2 = 0.480$, $p = 0.0087$).

We also assessed spreading of all cells using both individual cell circularity and projected area covered by all cells in phalloidin stained samples. No differences in circularity or spreading were noted 1 d after seeding (Figure S4). After 7 d, average circularity decreased in all gels (Figure S4A, $p < 0.0001$) and area coverage increased (Figure S4B, $p < 0.005$), but this effect was most pronounced in 27 mg/mL gels ($p = 0.033$ relative to 40 mg/mL).

In contrast to co-culture experiments, ECs cultured in the absence of DFs did not undergo capillary morphogenesis (Figure 2A). The shear moduli of EC or DF monocultures in 27 mg/mL hydrogels were statistically unchanged after 7 d, similar to controls (Figure 2B). EC mono-culture cell densities significantly decreased 2.7-fold (Figure 2C, $p < 0.01$) and cell bodies remained rounded (Fig 2D), whereas DF mono-culture cell densities significantly increased 1.6-fold (Figure 2C, $p < 0.01$) and cell bodies appeared well spread (Figure 2E).

In addition to stiffening accompanying capillary morphogenesis, we observed that soft hydrogel constructs changed shape macroscopically, suggesting possible gel compaction (Figure S5). To investigate whether compaction could account for the apparent changes in modulus and vessel density, we entrapped 2 μm beads within the hydrogel network as fiduciary markers, allowing us to infer changes in hydrogel density from changes in bead density specifically in the centers of the gels were capillary density was measured. Incorporation of beads did not substantially alter initial hydrogel mechanical properties nor stiffening behavior (Figure S6A). As expected, after overnight swelling we observed a decrease in bead density to 34 ± 6 % of reference gels (Figure S6B), where density was quantified immediately after gelation. This result corresponded closely with the observed changes in cell density after gel swelling and confirmed the validity of the technique. Despite the suggestion of hydrogel compaction from macroscopic images for 27 mg/mL hydrogels, no significant differences in bead density (measured locally inside of the gels) were observed as a function of gel composition during the 7 d culture (Figure S6B), though a weak inverse correlation was noted between initial gel modulus and change in bead density from 1 d to 7 d (Figure S6C, $R^2 = 0.3935$, $p = 0.016$).

2) Active cellular contraction significantly contributes to hydrogel stiffening

To investigate the contribution of cell-generated forces to hydrogel stiffening, we blocked cell-mediated contractility with the myosin II inhibitor, blebbistatin. Only 27 and 32 mg/mL hydrogels were assessed because 40 mg/mL hydrogels did not stiffen. Gels were incubated with 30 μM blebbistatin for the final 24 h of a 7 d culture period to inhibit traction forces [26] and minimize confounding effects from changes in vessel density, nuclei density, and cell spreading that occur with long-term blebbistatin treatment [27, 28]. This treatment caused a significant decrease in measured modulus of 36 ± 6% and 30 ± 11% for 27 and 32 mg/mL hydrogels, respectively ($p < 0.030$, Figure 3A). Interestingly, the 32 mg/mL hydrogels relaxed back to their initial shear moduli whereas the 27 mg/mL hydrogels did not (Figures 1B, 3A), suggesting our softest gels may incur some degree of permanent remodeling. 24-hour treatment with blebbistatin did not cause any changes in vessel density (Figure 3B), nuclei density (Figure 3C), or cell-spread coverage (Figure 3D), but did cause a modest increase in circularity in 27 mg/mL hydrogels ($p = 0.015$, Figure 3E), suggesting some retraction of cellular protrusions occurred without significantly altering average cell

size. 24-hour blebbistatin treatment did not affect gel density as assessed by microbead density (Figure 3F). In contrast, supplementing blebbistatin daily over the entire 7d culture period resulted in the dissolution of 27 mg/mL gels and significant softening for 32 mg/mL gels ($p = 0.0015$, Figure S7A), as well as significantly reduced vessel density and cell density ($p \leq 0.017$, Figure S7B–D).

To investigate if initial matrix stiffness alters cell phenotypes associated with increased cellular contractility [29], we measured ACTA2 (α-smooth muscle actin, αSMA) gene expression. The expression of αSMA was significantly upregulated in all constructs during culture, but the increase was most significant for the 27 mg/mL gels ($p = 0.017$ relative to 40 mg/mL, Figure 4A). Immunofluorescent staining showed that αSMA was expressed exclusively in UEA negative fibroblasts, which were often present in the perivascular space (Figure 4B) and appeared in all gel formulations (Figure S8). The pooled RNA contained transcripts from both cell types but αSMA is only expressed in fibroblasts. Therefore, the measured increase in αSMA expression could either represent an increase in αSMA per fibroblast or a higher proportion of fibroblasts contributing to the RNA pool. To differentiate these possibilities, we estimated the proportion of fibroblasts in our samples by quantifying the number of nuclei excluded from UEA stained regions. There was not an increased proportion of fibroblasts in soft hydrogel formulations (Figure 4C), demonstrating that soft hydrogels supported higher levels of αSMA expression in fibroblasts.

3) Enhanced deposition of collagen I and downregulation of MMP expression associates with hydrogel stiffening in ultra-soft hydrogels

The observation that blebbistatin inhibition of cell-mediated contractility did not result in a return to initial mechanical properties in 27 mg/mL gels suggested deposition of new matrix may contribute to stiffening. To assess this possibility, we quantified mRNA levels of collagen I alpha 1 chain (COL1A1), fibronectin (FN1), laminin beta 1 chain (LAMB1), and collagen IV alpha 1 chain (COL4A1) in pooled RNA collected from both cell populations in the gels. No differences in expression level were detected between hydrogels on day 1 (Figure 5). However, after 7 d of culture, we observed a 1.8-fold increase in collagen I expression in 27 mg/mL hydrogels compared with 40 mg/mL hydrogels ($p = 0.0007$, Figure 5). We also observed fibronectin expression in all gels was increased from 1 d to 7 d (Two-way ANOVA: time $p = 0.0002$, PEG $p = 0.11$, interaction $p = 0.0094$) but was most strongly upregulated in 40 mg/mL at day 7 ($p \leq 0.0009$). Expression of transcripts for the basement membrane component laminin beta 1 chain was unchanged during culture for the 27 mg/mL gels but was modestly upregulated 1.3-fold in 40 mg/mL gels ($p \leq 0.0021$). Collagen IV alpha 1 was upregulated after 7 d but did not depend on PEG composition.

We further analyzed the deposition of proteins encoded by these transcripts using immunostaining. Collagen I and fibronectin were deposited around both UEA negative fibroblasts and UEA positive vessels (Figure 6, Figure S9A). Compared with 27 mg/mL gels, we noted a qualitative decrease in Collagen I deposition in 40 mg/mL hydrogels, consistent with the expression analysis. Fibronectin deposition was observed not only around vessel like structures but also surrounding rounded cells which did not spread. In contrast to deposition of collagen I and fibronectin, the basement membrane proteins

laminin (beta 1 chain) and collagen IV (which reacts with both alpha 1 and alpha 2 chains) were tightly associated with UEA+ vessel-like structures and were less prominently expressed in UEA negative fibroblasts (Figure S9B, C). To assess the spatial distribution of ECM protein deposition relative to the encapsulated cells, we co-stained phalloidin with collagen I or fibronectin. In 27 mg/mL gels we observed very little ECM protein deposition in the hydrogel bulk distant from cells, with nearly all ECM deposited within ~30 μm of cells (Figure S10). We also noted areas of extensive ECM deposition devoid of actin but adjacent to nearby cells, suggesting active cellular remodeling in these regions followed by migration (Figure S10, arrowheads). Fibronectin expression surrounding poorly spread cells never extended more than a few microns from the nuclei.

Concurrent with our observation of enhanced matrix deposition in ultra-soft hydrogel formulations, we also observed downregulation of MT1-MMP and MMP2 in 27 mg/mL hydrogels compared to 40 mg/mL hydrogels on day 7 (Figure 7A, B, $p \leq 0.014$). However, there was no significant change in MMP9 expression over time regardless of formulation (Figure 7C).

4) Inhibition of matrix metalloproteinase (MMP)-mediated proteolysis reduces hydrogel stiffening and correlates with decreased cell spreading but not changes in cell number

We have previously shown that inhibition of MMPs with the broad-spectrum MMP inhibitor GM6001 severely restricts capillary morphogenesis in VPMS crosslinked hydrogels [5]. Given that our results to this point suggested stiffening behavior was due to cell contractility and pericellular matrix remodeling, we reasoned that blocking cell-mediated hydrogel degradation, needed for cell spreading and endothelial tube assembly, would also abolish gel stiffening. Closely mirroring the decrease in vessel density with GM6001 which we previously reported [5], we observed a robust and dose-dependent loss of gel stiffening with GM6001 (Figure 8A) in comparatively soft 32 mg/mL hydrogels (30 ± 8 Pa on day 1). Notably, GM6001 did not significantly alter cell density in the gels, indicating changes in stiffening were not due to reduced cell density over time (Figure 8B). We measured a significant rise in circularity with increasing doses of GM6001 (ANOVA: $p < 0.0001$, Figure 8C) and a non-significant trend toward lower cell coverage (Figure 8D), both suggesting reduced cell spreading with GM6001.

DISCUSSION

While the effects of stiffness on capillary morphogenesis have been studied extensively [20], how cells, in turn, alter the mechanical properties of their surrounding ECM during this process has received less attention [19]. A clear understanding of the dynamic and reciprocal relationship between cells and their mechanical microenvironment is critical to engineer synthetic materials for regenerative medicine applications because these mechanical changes may in turn affect the differentiation and function of co-encapsulated functional cell types [13]. Protease-susceptible PEG hydrogels are prototypical synthetic materials and have been widely utilized for their ability to support and control populations of single cells in 3D [30, 31]. However, the impact of their amorphous structure, which is distinct from native fibrillar ECMs, on complex multicellular morphogenetic processes remains less understood.

Consistent with several previous reports in other synthetic hydrogels, including protein-synthetic hybrid systems [32, 33] and polysaccharide-synthetic systems [22, 34], we observed enhanced vessel formation with reduced PEG crosslinking density [6, 8, 12, 23, 35]. Interestingly, this enhanced vessel formation in softer gel formulations was not correlated with differential expression of pro-angiogenic genes. However, the more surprising observation was that ultra-soft amorphous gels significantly stiffened over time as capillary morphogenesis occurred. We then used a combination of inhibitor studies and molecular expression analyses to provide evidence that both cell-mediated contractility and ECM deposition, but not hydrogel compaction, contribute to this stiffening. We then demonstrated that inhibition of cell-mediated degradation inhibited cellular spreading and severely attenuated gel stiffening.

We recently reported that fibrin matrices stiffen on both the microscale and the macroscale as capillary morphogenesis occurs [19], but it was not clear if this phenomenon required a fibrillar matrix to transduce cell-generated forces and thereby alter the mechanical microenvironment. The strain stiffening properties of fibrous materials such as fibrin and collagen allow cell-mediated tension to transmit mechanical forces over long distances, perhaps serving as a cue to guide network organization [15, 16, 36]. However, the nanoscale, amorphous architecture of PEG hydrogels is distinctly different from fibrin or collagen [21]. Such synthetic hydrogels generally display linear elastic deformation [36], which limits the distance mechanical forces can propagate relative to strain-stiffening fibrous materials.

To our knowledge, stiffening behavior in a purely synthetic matrix material during capillary morphogenesis has not been previously reported. Cell-mediated changes to hydrogel mechanics have, however, been more extensively studied in the context of fibrosis and wound healing, and engineering of load bearing tissues such as cartilage and bone [37]. Fibroblast-mediated stiffening of fibrous materials is well documented in fibrin [19] and collagen [38], is dependent on cellular contractility, and results in hydrogel compaction [39]. Dermal fibroblasts have also been shown to stiffen and compact PEG-fibrinogen composites [40]. However, we did not observe a significant change in marker bead density over time depending on gel formulation, suggesting that gel compaction was not necessarily associated with stiffening in our system. These observations suggest the bulk of PEG gels are not significantly reorganized, unlike collagen or fibrin which restructure into more compact fibrous architectures [41]. Distinct from fibrillar ECM or PEG-fibrinogen composite hydrogels, we also observed that stiffening depended on the co-culture of ECs with DFs. In the absence of capillary morphogenesis, DFs failed to stiffen ultra-soft hydrogel formulations. In contrast, others have reported that fibroblasts in unmodified alginate [42] and endothelial colony forming cells in RGD modified hyaluronan crosslinked with MMP degradable peptides [43] soften over time. These differences in the evolution of hydrogel mechanics depending on cell culture system demonstrate a complex interplay between cell types and ECM identity in dictating changes to hydrogel mechanics over time.

The cellular networks that formed throughout the bulk of the hydrogel may themselves be mediating the stiffening effects via cell-mediated contractility. To test this hypothesis, we included a saturating dose of blebbistatin, which inhibits the action of myosin II [44], in our culture medium for the final 24 hours of culture. This treatment reversed about half of the

observed stiffening in the 27 mg/mL and all the stiffening seen in the 32 mg/mL gels, implicating cytoskeletal tension as a major contributor to the observed stiffening behavior. We previously demonstrated that long term inhibition of cell-mediated contractility severely attenuated endothelial sprouting in fibrin [27]. Likewise, we observed that exposure to blebbistatin throughout the 7 d culture period not only reduced capillary morphogenesis, but resulted in gel softening over time. Matrix stiffness itself may also directly impact the degree of cellular contractility. Mabry *et al.* observed that valvular interstitial cells exhibited a more contractile phenotype in soft materials and that this phenotype could be reversed by changing matrix mechanics in situ [45]. Likewise, we observed an increase in the expression of α-smooth muscle actin in fibroblasts within our soft hydrogel constructs during capillary morphogenesis.

Since 24-hour exposure to blebbistatin did not fully reverse stiffening in the softest gels, the contributions of matrix deposition to the observed stiffening behavior were also assessed. We observed that collagen I alpha 1 chain was upregulated in pooled RNA samples from the soft hydrogels. Collagen I alpha chain is one of the key secreted proteins from fibroblasts that induce capillary morphogenesis in coculture with endothelial cells and its deposition contributes to progressive stiffening of fibrin [46]. Deposition of ECM proteins by chondrocytes in alginate has similarly been correlated with progressive hydrogel stiffening [47]. We noted collagen I near both vessels and fibroblasts but not within the bulk of the PEG hydrogels, suggesting deposition was highly localized. Fibronectin was also upregulated in all gel formulations and was deposited in a clear pericellular distribution around cells, similar to that of collagen I, as has been reported previously [8]. We also observed decreased expression of MT1-MMP and MMP2 in ultra-soft hydrogels which would shift ECM dynamics toward deposition over degradation.

Combined, the tight association of ECM proteins with invading cells, lack of change in the bulk hydrogel density, and the dependence of stiffening on cell contractility suggested a model in which networks of cells deposit an interconnected fibrillar architecture in soft hydrogels. Such a network also provides a mechanism for long-range force transmission that may help to facilitate network organization in the otherwise amorphous material. This network could result in a composite with properties increasingly dominated by a relatively stiff network of cells and their pericellular ECM rather than the adjacent soft amorphous hydrogel material. Cell-mediated tension may contribute to hydrogel mechanics by propagating through this newly deposited ECM and possibly through endothelial tubules themselves, which has been suggested in fibrin hydrogels [28]. This suggests that co-culture of ECs and DFs in PEG may be necessary to induce formation of a sufficiently interconnected network through which traction forces can propagate.

In support of our hypothesis that cellular network formation is necessary to allow hydrogel stiffening, we also observed a profound loss of stiffening behavior in co-cultures containing the MMP inhibitor GM6001, which inhibits MMP-mediated proteolysis necessary for cell spreading. Cell-mediated matrix degradation is required for an interconnected network of cells to form and deposit ECM. MMPs are required for capillary morphogenesis in natural ECMs [48, 49] and MMP-degradable PEG hydrogels [5, 6], but our findings here show they are also required for stiffening in a synthetic hydrogel. This effect may be MMP-specific

because inhibition of plasmin-mediated degradation in PEG-fibrinogen hydrogels was necessary to permit stiffening [40]. Moreover, our results suggest that cellular growth and deposition of new ECM outpaces global proteolytic hydrogel degradation in this model tissue.

Reciprocal crosstalk between ECM stiffness and cell-mediated remodeling to adjust the cellular microenvironment has been suggested in the progression of tumors [13] and may also partially regulate the process of neovascularization. Here we demonstrate a correlation between gel stiffening and capillary morphogenesis, suggesting that localized cellular remodeling around networks of fibroblasts and ECs is necessary for both processes to occur. Therefore, these data suggest that the initial mechanical properties of the cellular microenvironment may not directly dictate capillary morphogenesis *per se*, but instead create a permissive environment that can be readily remodeled by the cells themselves. This hypothesis is supported by observations by Sokic *et al.* that capillary morphogenesis is significantly enhanced in PEG hydrogels with similar initial mechanical properties but with MMP degradability controlled by crosslinking peptide sequence [23]. Counterintuitively, this suggests that enhancing MMP degradability may also result in enhanced hydrogel stiffening.

In summary, this study highlights the critical importance of cell-mediated remodeling on the evolution of tissue-level mechanical properties during the complex multicellular process of capillary morphogenesis in 3D. ECM mechanics affect the differentiation and function of many target cell types in engineered tissues beyond ECs and fibroblasts, such as osteoblasts, neurons, hepatocytes, and renal epithelium [50, 51]. Thus, dynamic changes in matrix properties are a particularly important consideration in the design of functional vascularized tissues formed from multiple cell types to ensure the mechanical environment is permissive both for the morphogenesis of vascular structures and for tissue function. Characterizing cell-mediated changes to hydrogel mechanics provides an essential framework for understanding, and ultimately controlling, the evolution of tissue mechanics when applied for regenerative medicine applications.

Supplementary Material

Refer to Web version on PubMed Central for supplementary material.

ACKNOWLEDGEMENTS

Research reported in this publication was supported by the National Heart, Lung, and Blood Institute of the National Institutes of Health under Award Number R01-HL085339. JAB was partially supported by the Kidney Research Training Program (T32-DK007378). BAJ was partially supported by the Tissue Engineering and Regeneration Training Program at the University of Michigan (T32-DE007057) and by the Training Program in Translational Cardiovascular Research and Entrepreneurship (T32-HL125242). The content is solely the responsibility of the authors and does not necessarily represent the official views of the National Institutes of Health. The authors confirm that there are no known conflicts of interest associated with this publication and there has been no significant financial support for this work that could have influenced its outcome.

REFERENCES

[1]. Blache U, Ehrbar M, Inspired by Nature: Hydrogels as Versatile Tools for Vascular Engineering, Adv Wound Care (New Rochelle) 7(7) (2018) 232–246. [PubMed: 29984113]

[2]. Rouwkema J, Khademhosseini A, Vascularization and Angiogenesis in Tissue Engineering: Beyond Creating Static Networks, Trends Biotechnol 34(9) (2016) 733–745. [PubMed: 27032730]

[3]. Allen P, Melero-Martin J, Bischoff J, Type I collagen, fibrin and PuraMatrix matrices provide permissive environments for human endothelial and mesenchymal progenitor cells to form neovascular networks, J Tissue Eng Regen Med 5(4) (2011) e74–86. [PubMed: 21413157]

[4]. Lin CC, Anseth KS, PEG hydrogels for the controlled release of biomolecules in regenerative medicine, Pharm Res 26(3) (2009) 631–43. [PubMed: 19089601]

[5]. Beamish JA, Juliar BA, Cleveland DS, Busch ME, Nimmagadda L, Putnam AJ, Deciphering the relative roles of matrix metalloproteinase- and plasmin-mediated matrix degradation during capillary morphogenesis using engineered hydrogels, J Biomed Mater Res B Appl Biomater (2019).

[6]. Vigen M, Ceccarelli J, Putnam AJ, Protease-sensitive PEG hydrogels regulate vascularization in vitro and in vivo, Macromol Biosci 14(10) (2014) 1368–79. [PubMed: 24943402]

[7]. Leslie-Barbick JE, Saik JE, Gould DJ, Dickinson ME, West JL, The promotion of microvasculature formation in poly(ethylene glycol) diacrylate hydrogels by an immobilized VEGF-mimetic peptide, Biomaterials 32(25) (2011) 5782–9. [PubMed: 21612821]

[8]. Blache U, Vallmajo-Martin Q, Horton ER, Guerrero J, Djonov V, Scherberich A, Erler JT, Martin I, Snedeker JG, Milleret V, Ehrbar M, Notch-inducing hydrogels reveal a perivascular switch of mesenchymal stem cell fate, EMBO Rep (2018).

[9]. Schweller RM, West JL, Encoding Hydrogel Mechanics via Network Cross-Linking Structure, ACS Biomaterials Science & Engineering 1(5) (2015) 335–344. [PubMed: 26082943]

[10]. Phelps EA, Templeman KL, Thulé PM, García AJ, Engineered VEGF-releasing PEG–MAL hydrogel for pancreatic islet vascularization, Drug Delivery and Translational Research 5(2) (2015) 125–136. [PubMed: 25787738]

[11]. Tsurkan MV, Chwalek K, Prokoph S, Zieris A, Levental KR, Freudenberg U, Werner C, Defined polymer-peptide conjugates to form cell-instructive starPEG-heparin matrices in situ, Adv Mater 25(18) (2013) 2606–10. [PubMed: 23576312]

[12]. Moon JJ, Saik JE, Poche RA, Leslie-Barbick JE, Lee SH, Smith AA, Dickinson ME, West JL, Biomimetic hydrogels with pro-angiogenic properties, Biomaterials 31(14) (2010) 3840–7. [PubMed: 20185173]

[13]. Xu R, Boudreau A, Bissell MJ, Tissue architecture and function: dynamic reciprocity via extra- and intra-cellular matrices, Cancer Metastasis Rev 28(1-2) (2009) 167–76. [PubMed: 19160017]

[14]. Davis GE, Norden PR, Bowers SL, Molecular control of capillary morphogenesis and maturation by recognition and remodeling of the extracellular matrix: functional roles of endothelial cells and pericytes in health and disease, Connect Tissue Res 56(5) (2015) 392–402. [PubMed: 26305158]

[15]. Davis GE, Camarillo CW, Regulation of Endothelial Cell Morphogenesis by Integrins, Mechanical Forces, and Matrix Guidance Pathways, Experimental Cell Research 216(1) (1995) 113–123. [PubMed: 7813611]

[16]. Ceccarelli J, Cheng A, Putnam AJ, Mechanical strain controls endothelial patterning during angiogenic sprouting, Cellular and molecular bioengineering 5(4) (2012) 463–473. [PubMed: 24015155]

[17]. Davidson CD, Wang WY, Zaimi I, Jayco DKP, Baker BM, Cell force-mediated matrix reorganization underlies multicellular network assembly, Sci Rep 9(1) (2019) 12.

[18]. Kniazeva E, Weidling JW, Singh R, Botvinick EL, Digman MA, Gratton E, Putnam AJ, Quantification of local matrix deformations and mechanical properties during capillary morphogenesis in 3D, Integrative Biology 4(4) (2012) 431–439. [PubMed: 22281872]

[19]. Juliar BA, Keating MT, Kong YP, Botvinick EL, Putnam AJ, Sprouting angiogenesis induces significant mechanical heterogeneities and ECM stiffening across length scales in fibrin hydrogels, Biomaterials (2018).

[20]. LaValley DJ, Reinhart-King CA, Matrix stiffening in the formation of blood vessels, Advances in Regenerative Biology 1(0) (2014).

[21]. Raeber GP, Lutolf MP, Hubbell JA, Molecularly Engineered PEG Hydrogels: A Novel Model System for Proteolytically Mediated Cell Migration, Biophysical Journal 89(2) (2005) 1374–1388. [PubMed: 15923238]

[22]. Chwalek K, Tsurkan MV, Freudenberg U, Werner C, Glycosaminoglycan-based hydrogels to modulate heterocellular communication in in vitro angiogenesis models, Sci Rep 4 (2014) 4414. [PubMed: 24643064]

[23]. Sokic S, Papavasiliou G, Controlled Proteolytic Cleavage Site Presentation in Biomimetic PEGDA Hydrogels Enhances Neovascularization In Vitro, Tissue Engineering Part A 18(23-24) (2012) 2477–2486. [PubMed: 22725267]

[24]. Ghajar CM, Blevins KS, Hughes CC, George SC, Putnam AJ, Mesenchymal stem cells enhance angiogenesis in mechanically viable prevascularized tissues via early matrix metalloproteinase upregulation, Tissue Eng 12(10) (2006) 2875–88. [PubMed: 17518656]

[25]. Lutolf MP, Lauer-Fields JL, Schmoekel HG, Metters AT, Weber FE, Fields GB, Hubbell JA, Synthetic matrix metalloproteinase-sensitive hydrogels for the conduction of tissue regeneration: Engineering cell-invasion characteristics, Proceedings of the National Academy of Sciences 100(9) (2003) 5413–5418.

[26]. Beningo KA, Hamao K, Dembo M, Wang YL, Hosoya H, Traction forces of fibroblasts are regulated by the Rho-dependent kinase but not by the myosin light chain kinase, Arch Biochem Biophys 456(2) (2006) 224–31. [PubMed: 17094935]

[27]. Kniazeva E, Putnam AJ, Endothelial cell traction and ECM density influence both capillary morphogenesis and maintenance in 3-D, American Journal of Physiology - Cell Physiology 297(1) (2009).

[28]. Rosenfeld D, Landau S, Shandalov Y, Raindel N, Freiman A, Shor E, Blinder Y, Vandenburgh HH, Mooney DJ, Levenberg S, Morphogenesis of 3D vascular networks is regulated by tensile forces, Proceedings of the National Academy of Sciences 113(12) (2016) 321-3220-3220.

[29]. Hinz B, Phan SH, Thannickal VJ, Prunotto M, Desmouliere A, Varga J, De Wever O, Mareel M, Gabbiani G, Recent developments in myofibroblast biology: paradigms for connective tissue remodeling, Am J Pathol 180(4) (2012) 1340–55. [PubMed: 22387320]

[30]. Zhu J, Bioactive modification of poly(ethylene glycol) hydrogels for tissue engineering, Biomaterials 31(17) (2010) 4639–56. [PubMed: 20303169]

[31]. Murphy WL, McDevitt TC, Engler AJ, Materials as stem cell regulators, Nat Mater 13(6) (2014) 547–57. [PubMed: 24845994]

[32]. Singh RK, Seliktar D, Putnam AJ, Capillary morphogenesis in PEG-collagen hydrogels, Biomaterials 34(37) (2013) 9331–9340. [PubMed: 24021759]

[33]. Chen YC, Lin RZ, Qi H, Yang Y, Bae H, Melero-Martin JM, Khademhosseini A, Functional Human Vascular Network Generated in Photocrosslinkable Gelatin Methacrylate Hydrogels, Adv Funct Mater 22(10) (2012) 2027–2039. [PubMed: 22907987]

[34]. Trappmann B, Baker BM, Polacheck WJ, Choi CK, Burdick JA, Chen CS, Matrix degradability controls multicellularity of 3D cell migration, Nature Communications 8(1) (2017) 371.

[35]. Zanotelli MR, Ardalani H, Zhang J, Hou Z, Nguyen EH, Swanson S, Nguyen BK, Bolin J, Elwell A, Bischel LL, Xie AW, Stewart R, Beebe DJ, Thomson JA, Schwartz MP, Murphy WL, Stable engineered vascular networks from human induced pluripotent stem cell-derived endothelial cells cultured in synthetic hydrogels, Acta Biomater 35 (2016) 32–41. [PubMed: 26945632]

[36]. Winer JP, Oake S, Janmey PA, Non-linear elasticity of extracellular matrices enables contractile cells to communicate local position and orientation, PLoS One 4(7) (2009) e6382. [PubMed: 19629190]

[37]. Ahearne M, Introduction to cell-hydrogel mechanosensing, Interface Focus 4(2) (2014) 20130038. [PubMed: 24748951]

[38]. Wakatsuki T, Elson EL, Reciprocal interactions between cells and extracellular matrix during remodeling of tissue constructs, Biophys Chem 100(1-3) (2003) 593–605. [PubMed: 12646393]

[39]. Meshel AS, Wei Q, Adelstein RS, Sheetz MP, Basic mechanism of three-dimensional collagen fibre transport by fibroblasts, Nat Cell Biol 7(2) (2005) 157–64. [PubMed: 15654332]

[40]. Kesselman D, Kossover O, Mironi-Harpaz I, Seliktar D, Time-dependent cellular morphogenesis and matrix stiffening in proteolytically responsive hydrogels, Acta Biomaterialia 9(8) (2013) 7630–7639. [PubMed: 23624218]

[41]. Jansen KA, Bacabac RG, Piechocka IK, Koenderink GH, Cells actively stiffen fibrin networks by generating contractile stress, Biophys J 105(10) (2013) 2240–51. [PubMed: 24268136]

[42]. Hunt NC, Smith AM, Gbureck U, Shelton RM, Grover LM, Encapsulation of fibroblasts causes accelerated alginate hydrogel degradation, Acta Biomater 6(9) (2010) 3649–56. [PubMed: 20307693]

[43]. Hanjaya-Putra D, Bose V, Shen Y-I, Yee J, Khetan S, Fox-Talbot K, Steenbergen C, Burdick JA, Gerecht S, Controlled activation of morphogenesis to generate a functional human microvasculature in a synthetic matrix, Blood 118(3) (2011) 804-815-815.

[44]. Kovacs M, Toth J, Hetenyi C, Malnasi-Csizmadia A, Sellers JR, Mechanism of blebbistatin inhibition of myosin II, J Biol Chem 279(34) (2004) 35557–63. [PubMed: 15205456]

[45]. Mabry KM, Lawrence RL, Anseth KS, Dynamic stiffening of poly(ethylene glycol)-based hydrogels to direct valvular interstitial cell phenotype in a three-dimensional environment, Biomaterials 49 (2015) 47–56. [PubMed: 25725554]

[46]. Newman AC, Nakatsu MN, Chou W, Gershon PD, Hughes CCW, The requirement for fibroblasts in angiogenesis: fibroblast-derived matrix proteins are essential for endothelial cell lumen formation, Molecular Biology of the Cell 22(20) (2011) 3791–3800. [PubMed: 21865599]

[47]. Williams GM, Klein TJ, Sah RL, Cell density alters matrix accumulation in two distinct fractions and the mechanical integrity of alginate-chondrocyte constructs, Acta Biomater 1(6) (2005) 625–33. [PubMed: 16701843]

[48]. Hiraoka N, Allen E, Apel IJ, Gyetko MR, Weiss SJ, Matrix Metalloproteinases Regulate Neovascularization by Acting as Pericellular Fibrinolysins, Cell 95(3) (1998) 365–377. [PubMed: 9814707]

[49]. Ghajar CM, George SC, Putnam AJ, Matrix metalloproteinase control of capillary morphogenesis, Critical reviews in eukaryotic gene expression 18(3) (2008) 251–278. [PubMed: 18540825]

[50]. Eyckmans J, Boudou T, Yu X, Chen CS, A hitchhiker's guide to mechanobiology, Dev Cell 21(1) (2011) 35–47. [PubMed: 21763607]

[51]. Beamish JA, Chen E, Putnam AJ, Engineered extracellular matrices with controlled mechanics modulate renal proximal tubular cell epithelialization, PLOS ONE 12(7) (2017).

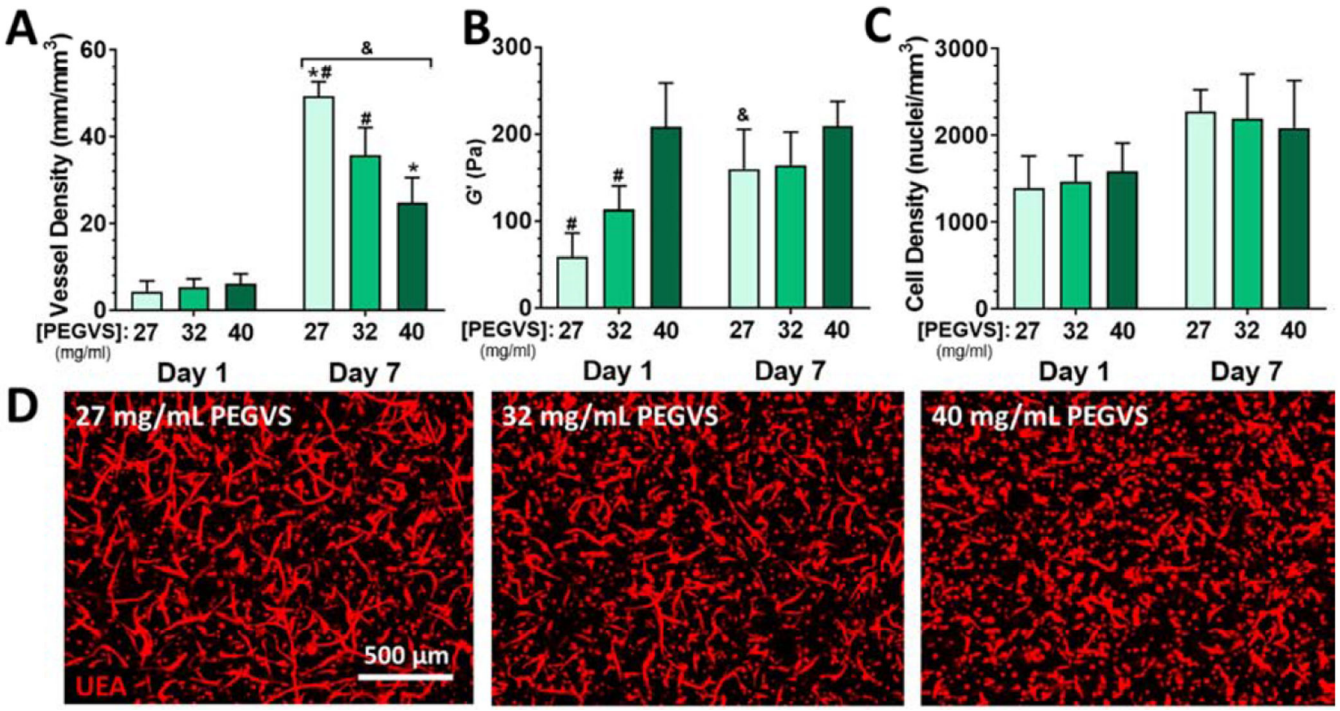

Figure 1: Lower concentration of PEGVS at the time of crosslinking results in higher vessel density at 7 d and induces gel stiffening without altering cell density.

A) Hydrogel constructs were formed with a range of concentrations of PEGVS and cultured for 7 d. Vessel density in the bulk of the constructs was estimated as described in the methods. B) The shear storage modulus (G') of constructs was determined after overnight culture (Day 1) and at 7 d. C) Cell density in the constructs after 1 d and 7 d was quantified from DAPI stained images. Two-way ANOVA: time $p < 0.001$, PEG $p > 0.99$, interaction $p = 0.60$. D) Representative images of maximum intensity projections of confocal sections (z height = 300 µm) for ECs stained with UEA at 7 d from constructs with a range of PEGVS compositions. #: $p < 0.05$, relative to 40 mg/mL PEGVS (same day); *: $p < 0.05$, relative to 32 mg/mL PEGVS (same day); &: $p < 0.05$ relative to day 1 (same PEGVS composition), N=4-7.

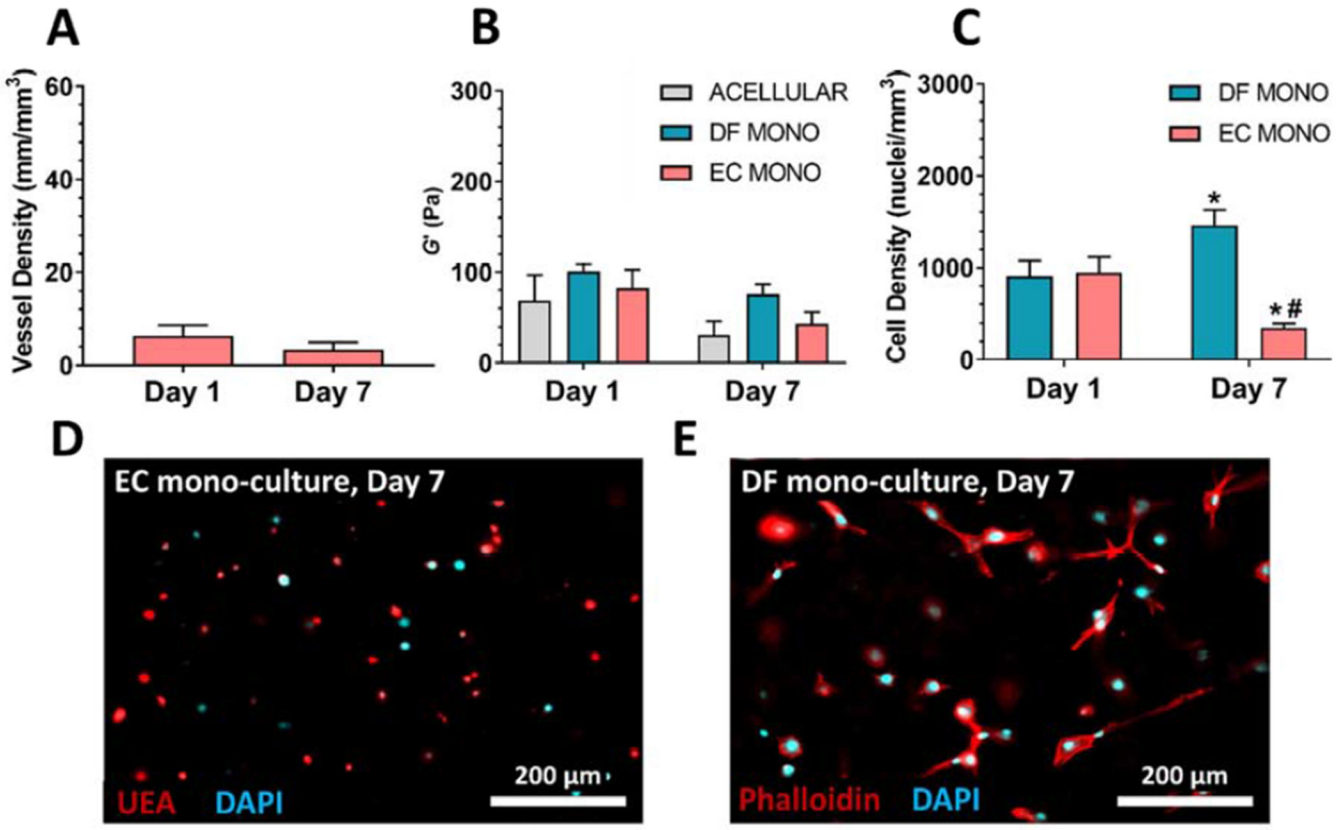

Figure 2: Co-culture of ECs with DFs is necessary for capillary morphogenesis and hydrogel stiffening.

A) ECs cultured in the absence of DFs in 27 mg/mL PEGVS did not develop capillary networks. B) The shear storage modulus (G') of 27 mg/mL constructs which were acellular or contained mono-cultures of either DFs or ECs did not show any significant differences between conditions on a given day or between days for a given condition. C) Mono-cultures of ECs in 27 mg/mL hydrogels demonstrated a significant decrease in nuclei density over a 7 d culture period and cell bodies remained rounded as visualized with UEA for cell bodies and DAPI for nuclei (D). Mono-cultures of DFs in 27 mg/mL hydrogels demonstrated a significant increase in nuclei density over a 7 d culture period (C) and cell bodies appeared well spread as visualized with phalloidin staining for cell bodies and DAPI for nuclei (E). *: $p < 0.05$, relative to Day 1 (same cellular condition). #: $p < 0.05$, relative to DF mono (same day); . Y-axes were scaled to match Fig. 1

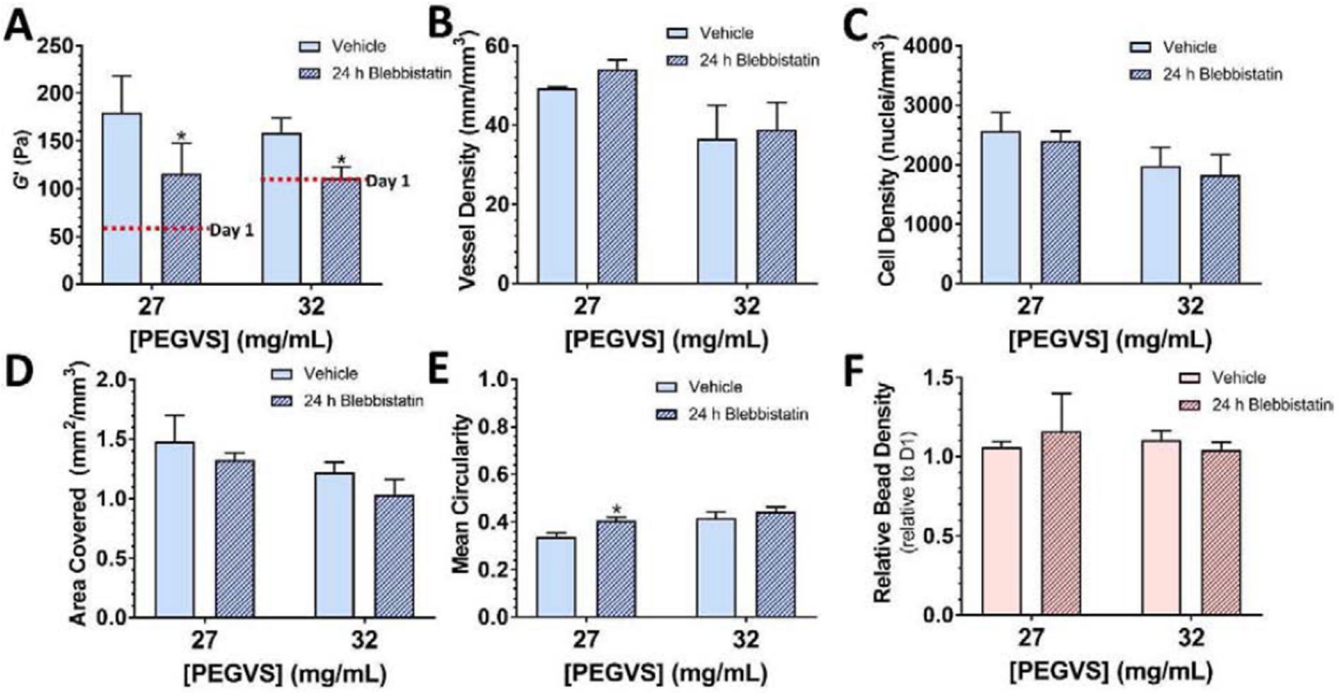

Figure 3: Cell contractility partly contributes to construct stiffening.

Hydrogel constructs with either 27 or 32 mg/mL PEGVS were cultured for 6 d and then were incubated with 30 μM blebbistatin or vehicle during the final 24 h of culture. The shear storage modulus (G') at 7 d was measured in each condition (A). Average stiffness at 1 d is shown in red on each graph for reference. 24 h treatment with blebbistatin did not affect vessel density (B), the cell density (C), or cell area covered (D). Blebbistatin induced a slight increase in cell circularity in 27 mg/mL PEGVS constructs (E). Blebbistatin did not alter the density of microbeads (F). *: $p < 0.05$, relative to vehicle control, N=3.

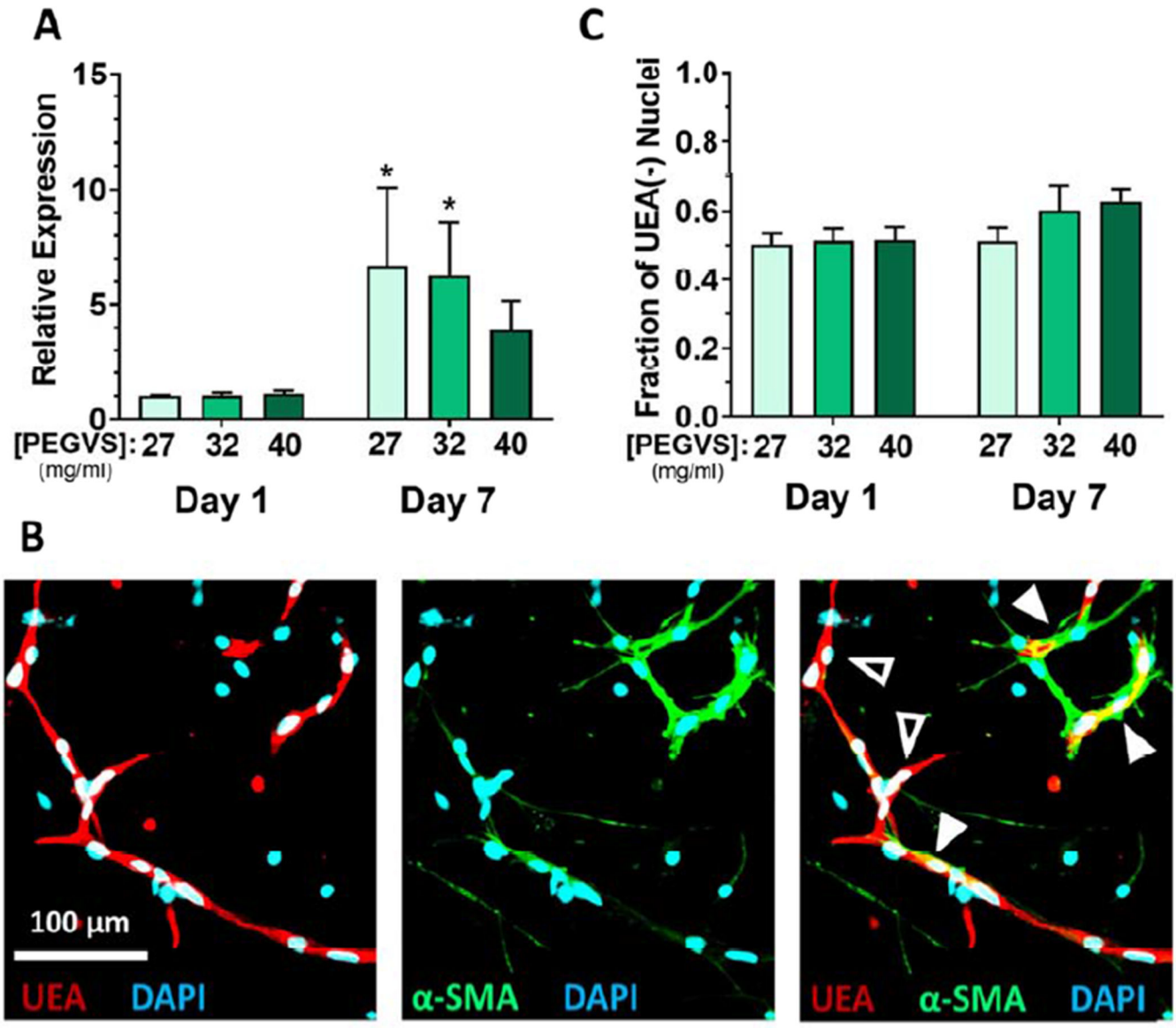

Figure 4: Smooth muscle actin is upregulated by fibroblasts in soft hydrogels.

A) Expression of α smooth muscle actin (αSMA, gene: ACTA2) was measured from RNA collected from constructs after 1 d or 7 d using real time RT-PCR. Expression levels were normalized to GAPDH in each sample and then to expression in 27 mg/mL PEGVS at 1 d ($\Delta\Delta C_t$ method). *: $p < 0.05$, relative to 40 mg/mL PEGVS, N=3. B) Only fibroblasts display significant α-smooth muscle actin protein expression. Representative image in an intermediate stiffness construct showing immunofluorescent staining for (αSMA), counterstained with UEA to highlight endothelium, and DAPI. Note the tight association of αSMA+ fibroblasts with UEA+ microvessels (solid arrowheads) but lack of αSMA staining in UEA+ microvessels themselves (open arrowhead). Scale bar = 100 µm. C) The proportion of UEA(−) nuclei (representing fibroblasts) in stiff constructs after 7 d was quantified as described in the supplemental methods.

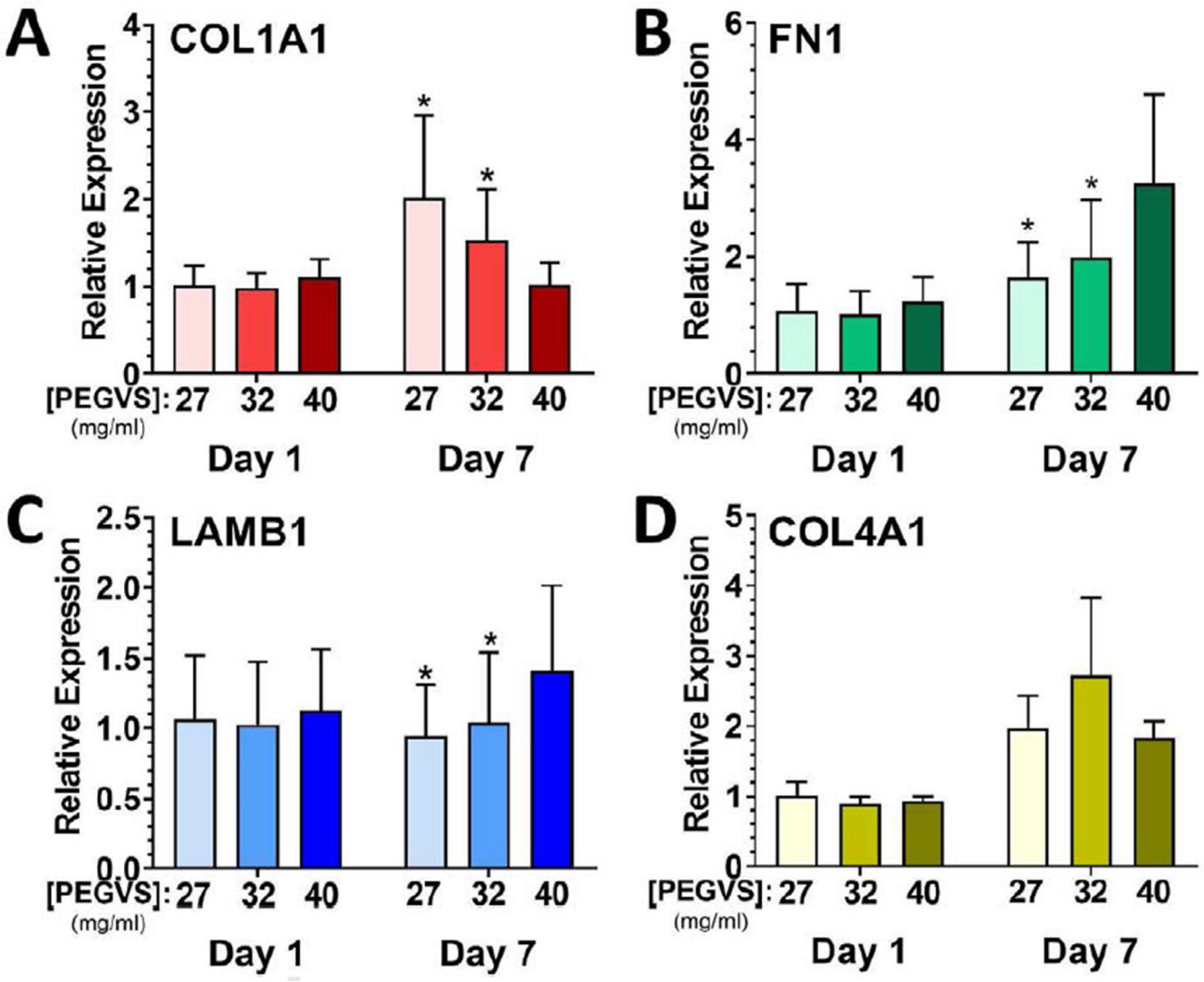

Figure 5: Collagen I alpha 1 chain expression is upregulated in soft hydrogels.

RNA was collected from constructs after 1 d and 7 d, purified, and expression determined using real time RT-PCR. Expression of collagen I α1 chain (COL1A1, A), fibronectin (FN1, B), laminin β1 chain (LAMB1, C), and collagen IV α1 chain (COL4A1, D) was measured. Expression levels were normalized to glyceraldehyde 3-phosphate dehydrogenase (GAPDH) in each sample and then to expression in 27 mg/mL PEGVS at 1 d ($\Delta\Delta C_t$ method). *: $p < 0.05$, relative to 40 mg/mL PEGVS same day, N=3.

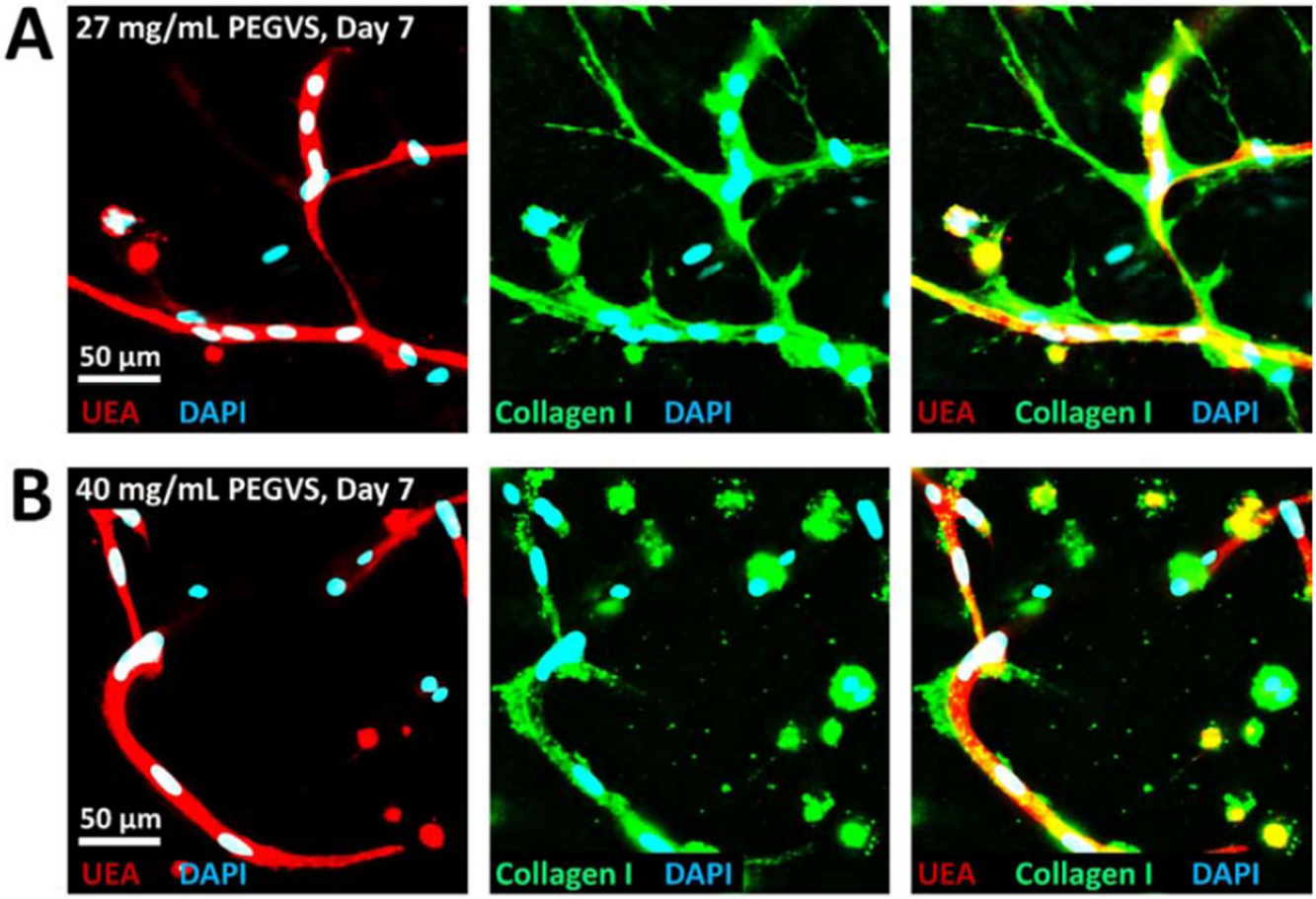

Figure 6: Collagen I deposition around vessels is more robust in soft hydrogels.

27 mg/mL (A) or 40 mg/mL (B) PEGVS constructs were fixed at 7d and stained for collagen I and counterstained with UEA and DAPI. There was a clear increase in collagen I deposition in 27 mg/mL constructs compared with 40 mg/mL.

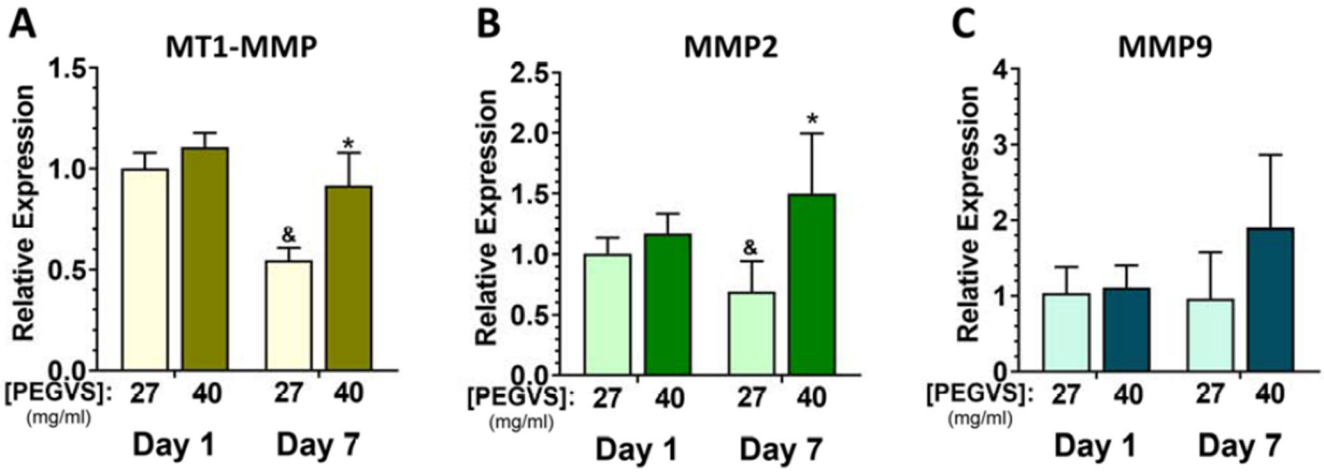

Figure 7: MMP expression is downregulated in ultra-soft hydrogel formulations.

RNA was collected from constructs after 1 d and 7 d, purified, and expression determined using real time RT-PCR. Expression of matrix type-1 MMP (MT1-MMP, A), MMP2 (B) and MMP9 (C) was measured. Expression levels were normalized to glyceraldehyde 3-phosphate dehydrogenase (GAPDH) in each sample and then to expression in 27 mg/mL PEGVS at 1 d ($\Delta\Delta C_t$ method). *: $p < 0.05$, relative to 27 mg/mL (same day); &: $p < 0.05$ relative to day 1 (same composition). N=3.

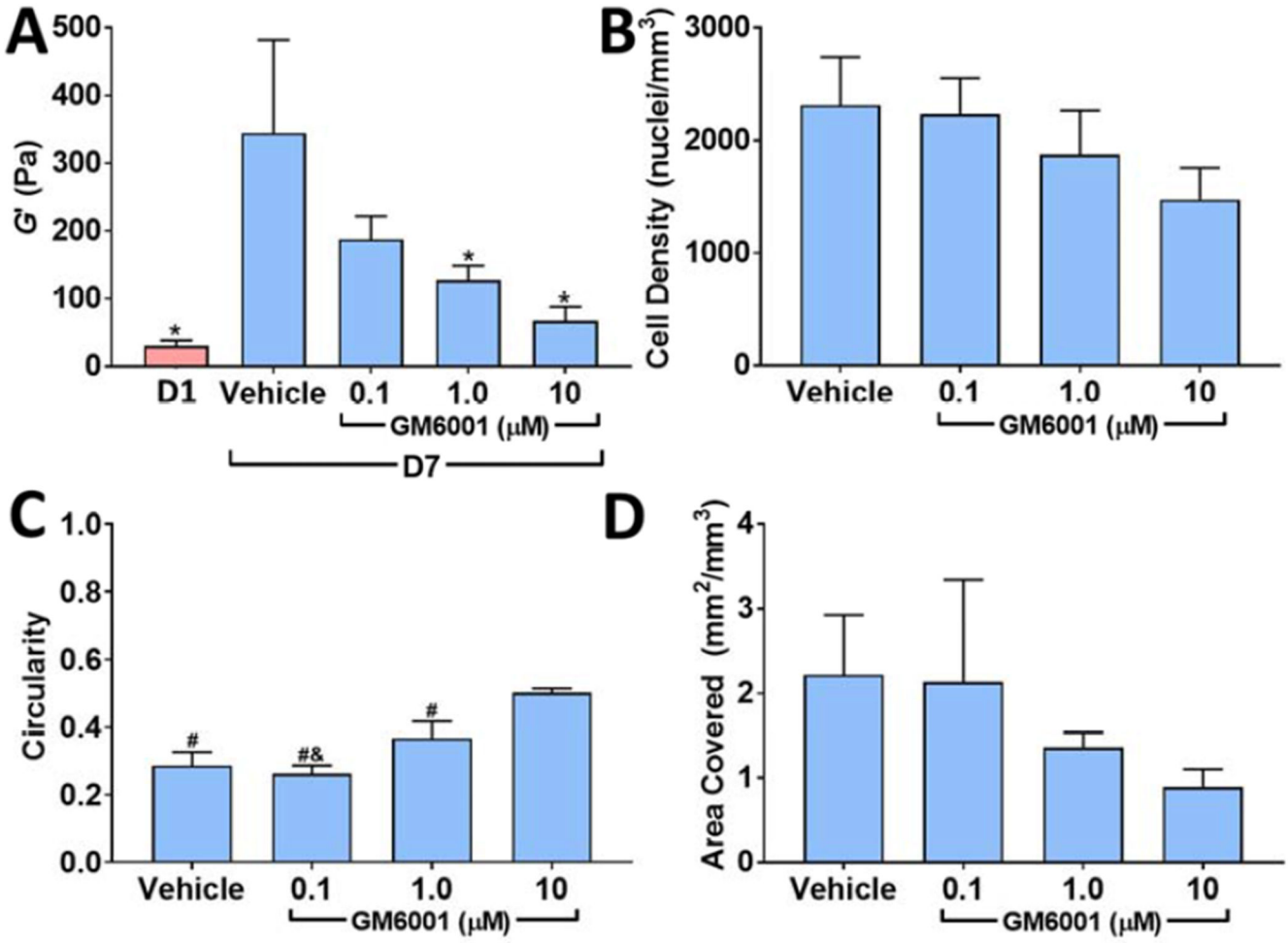

Figure 8. Inhibition of MMP-mediated matrix degradation abolishes gel stiffening and blocks cell spreading.

32 mg/mL PEGVS constructs were incubated with the broad-spectrum MMP inhibitor GM6001 for 7 d. The shear storage modulus (*G'*) at 7 d was measured in each condition (A, *: $p < 0.05$, relative to vehicle 7 d). There was a modest trend toward lower cell density with increasing GM6001 concentration but did not reach statistical significance (B, ANOVA: $p = 0.0734$). Average cell circularity, a measure of cell spreading, increased with GM6001 concentration (C, #: $p < 0.01$, relative to 10 μM GM6001; &: $p < 0.05$, relative to 1 μM GM6001, lower values of circularity reflect greater irregularly shaped spreading). Projected cell area covered also decreased with GM6001 concentration but did not reach statistical significance (D, ANOVA: $p = 0.1417$). N=3.